Tensor-guided interpolation on non-planar surfaces

Dave Hale
Center for Wave Phenomena, Colorado School of Mines, Golden CO 80401, USA

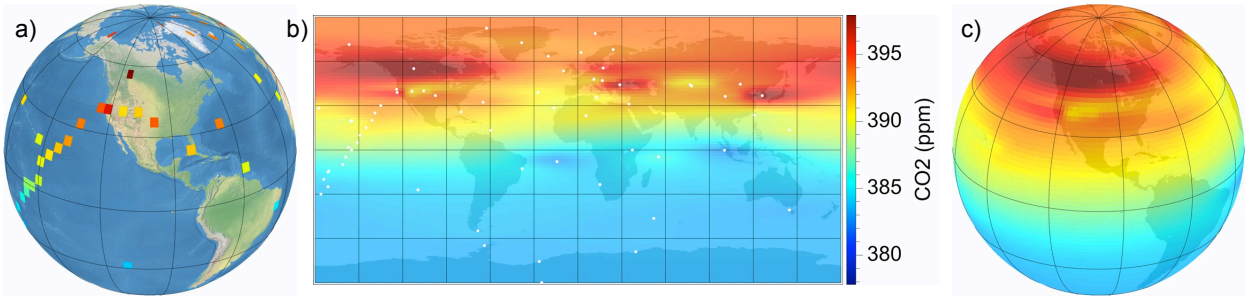

Figure 1. 65 monthly averages of atmospheric CO_2 measurements acquired at scattered locations on the earth's surface (a), and tensor-guided interpolation of those measurements in a 2D parametric space (b) to obtain interpolated CO_2 concentrations everywhere on that surface (c).

ABSTRACT

In blended-neighbor interpolation of scattered data, a tensor field represents a model of spatial correlation that is both anisotropic and spatially varying. In effect, this tensor field defines a non-Euclidean metric, a measure of distance that varies with direction and location. The tensors may be derived from secondary data, such as images.
Alternatively, when the primary data to be interpolated are measured on a non-planar surface, the tensors may be derived from surface geometry, and the non-Euclidean measure of distance is simply geodesic. Interpolation of geophysical data acquired on a non-planar surface should be consistent with tensor fields derived from both surface geometry and any secondary data.

Key words: tensor interpolation parametric surface

1 INTRODUCTION

Geophysical data are often acquired at locations scattered on surfaces that are not planar. For example, consider atmospheric CO_2 concentrations measured in flasks at locations scattered on the surface of the earth. The concentrations displayed in Figure 1a are monthly averages for April, 2009.

When interpolating such scattered data, as in Figures 1b and 1c, we are in effect estimating CO_2 concentrations that we have not measured. Today the most accurate method for doing this is inverse modeling, that is, to find carbon sources and sinks and use atmospheric transport models to obtain CO_2 concentrations that best match the values measured at scattered locations (e.g., Gurney et al., 2002). Inverse modeling is implemented by the CarbonTracker program (Peters et al., 2007) of the National Oceanic and Atmospheric Administration (NOAA).

This paper does not claim that the interpolation method used to compute CO_2 concentrations for Figure 1 is more accurate than inverse modeling. Rather, these CO_2 measurements simply illustrate the general problem of interpolating scattered data acquired on a surface that is not planar. This problem is ubiquitous in geophysics, and the interpolation method described in this paper may be useful for quick estimates or visualizations, and in contexts in which physical models or data are inadequate to enable an inverse modeling solution.

In the context of exploration geophysics, consider the interpolation of subsurface properties measured in boreholes at locations scattered within a geologic layer bounded by surfaces that are not planar. To simplify interpolation, we may attempt to flatten the layer and the bounding surfaces so that they are planar. However, such flattening may distort distances and, hence, spatial correlations within the layer (Lee, 2001). Flattening is unnecessary if we account directly for surface geometry in the method used to interpolate scattered data.

The interpolation method described in this paper is a simple extension of the image-guided blended neighbor interpolation method described by Hale (2009). This method interpolates scattered data using a tensor field derived from secondary information, such as a seismic image. In other words, image-guided interpolation is actually tensor-guided, and the tensors that guide interpolation can be derived from many sources, not only images.

This paper shows that the tensor-guided blended neighbor method is easily extended to interpolation on non-planar surfaces defined by a parametric mapping, because surface geometry simply alters the tensor field already employed by the method. Using the earth's surface as a familiar example, I demonstrate this method for honoring both surface geometry and secondary models for spatial correlation in the interpolation of data acquired at locations scattered on that surface.

2 TENSOR-GUIDED INTERPOLATION

Using the notation of Hale (2009), let us assume that spatially scattered data to be interpolated are a set

$$\mathcal{F} = \{f_1, f_2, \ldots, f_K\} \tag{1}$$

of K known sample values $f_k \in \mathbb{R}$ that correspond to a set

$$\mathcal{X} = \{\mathbf{x}_1, \mathbf{x}_2, \ldots, \mathbf{x}_K\} \tag{2}$$

of K known sample points $\mathbf{x}_k \in \mathbb{R}^n$. Together these two sets comprise a set

$$\mathcal{K} = \{(f_1, \mathbf{x}_1), (f_2, \mathbf{x}_2), \ldots, (f_K, \mathbf{x}_K)\} \tag{3}$$

of K known samples. These samples may be scattered such that the n-dimensional sample points in the set $\mathcal{X}$ may have no regular geometric structure. The classic interpolation problem is to use the known samples in $\mathcal{K}$ to construct a function $q(\mathbf{x}) : \mathbb{R}^n \to \mathbb{R}$, such that $q(\mathbf{x}_k) = f_k$.

As stated, this problem has no unique solution; there exist an infinite number of functions $q(\mathbf{x})$ that satisfy the interpolation conditions $q(\mathbf{x}_k) = f_k$. Additional criteria may include measures of smoothness, robustness, and computational efficiency. Because tradeoffs exist among such criteria, a variety of methods for interpolating scattered data are commonly used today.

In all of these methods the interpolation of spatially scattered data depends, either explicitly or implicitly, on a model for spatial correlation. In particular, correlation is often assumed to decrease with distance; measurements for any two nearby points tend to be more similar than those for two distant points. This dependence on a spatial correlation model is most explicit in statistical methods such as kriging that require the specification of covariance or variogram functions. These functions may be anisotropic, but are assumed to be stationary or at least slowly varying within neighborhoods of known samples. Geostatistical methods such as kriging are difficult to extend to contexts in which this stationarity assumption is invalid.

The interpolation method described in this paper depends explicitly on a model of spatial correlation that in practice is often highly anisotropic and spatially varying. This model is represented by a tensor field, and the interpolation is thereby *tensor-guided*.

The blended neighbor method (Hale, 2009) for interpolation was developed specifically to facilitate tensor-guided interpolation. This process consists of two steps:

Step 1: solve the eikonal equation

$$\begin{aligned} \boldsymbol{\nabla} t(\mathbf{x}) \bullet \mathbf{D}(\mathbf{x}) \bullet \boldsymbol{\nabla} t(\mathbf{x}) = 1, &\quad \mathbf{x} \notin \mathcal{X}; \\ t(\mathbf{x}_k) = 0, &\quad \mathbf{x}_k \in \mathcal{X} \end{aligned} \tag{4}$$

for

$t(\mathbf{x})$: the minimal time from $\mathbf{x}$ to the nearest known sample point $\mathbf{x}_k$, and
$p(\mathbf{x})$: the value f_k corresponding to the sample point $\mathbf{x}_k$ nearest to the point $\mathbf{x}$.

Step 2: solve the blending equation

$$q(\mathbf{x}) - \frac{1}{2}\boldsymbol{\nabla} \bullet t^2(\mathbf{x})\mathbf{D}(\mathbf{x}) \bullet \boldsymbol{\nabla} q(\mathbf{x}) = p(\mathbf{x}), \tag{5}$$

for the blended neighbor interpolant $q(\mathbf{x})$.

The tensor field in this method is denoted by $\mathbf{D}(\mathbf{x})$. At each location $\mathbf{x} \in \mathbb{R}^n$, the tensor $\mathbf{D}$ is a symmetric positive-definite $n \times n$ matrix. The tensor field $\mathbf{D}(\mathbf{x})$ provides a metric, a measure of distance that need not be Euclidean. Indeed, times $t(\mathbf{x})$ in equation 4 are actually non-Euclidean distances computed for the metric $\mathbf{D}(\mathbf{x})$.

We can get an intuitive sense of the metric $\mathbf{D}(\mathbf{x})$ by considering the special case where $\mathbf{D}$ is constant. In this case, the time (non-Euclidean distance) $t(\mathbf{x})$ from any known sample point $\mathbf{x}_k$ to an arbitrary point $\mathbf{x}$ can be computed analytically:

$$t = \sqrt{(\mathbf{x} - \mathbf{x}_k) \bullet \mathbf{D}^{-1} \bullet (\mathbf{x} - \mathbf{x}_k)}, \tag{6}$$

or in matrix-vector notation

$$t = \sqrt{(\mathbf{x} - \mathbf{x}_k)^T \mathbf{D}^{-1} (\mathbf{x} - \mathbf{x}_k)}. \tag{7}$$

One can easily verify by substitution that this expres-

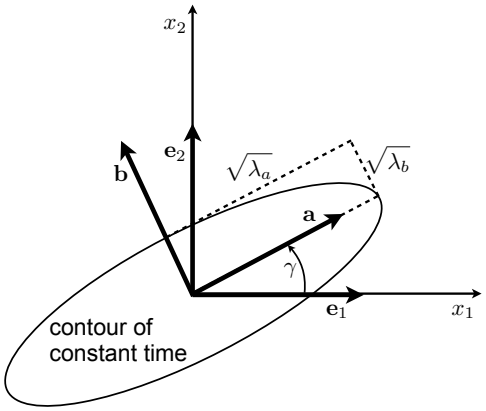

Figure 2. For a metric $\mathbf{D}(\mathbf{x})$, contours of constant time (non-Euclidean distance) within any infinitesimal neighborhood of a point $\mathbf{x}$ are elliptical. At each location $\mathbf{x}$, the ellipse is elongated in the direction in which spatial correlation is highest.

sion is a solution to the eikonal equation 4, here expressed in matrix-vector notation:

$$\boldsymbol{\nabla} t^T \mathbf{D} \boldsymbol{\nabla} t = 1, \tag{8}$$

with boundary condition $t(\mathbf{x}_k) = 0$.

For the general case where $\mathbf{D}(\mathbf{x})$ is spatially varying, we must compute the solution $t(\mathbf{x})$ of the eikonal equation 4 numerically. However, even in this case we may consider an infinitesimally small neighborhood of any location $\mathbf{x}$, in which $\mathbf{D}(\mathbf{x})$ is essentially constant, and the infinitesimal time $\mathrm{d}t$ from $\mathbf{x}$ to $\mathbf{x} + \mathrm{d}\mathbf{x}$ is

$$\mathrm{d}t = \sqrt{\mathrm{d}\mathbf{x}^T \mathbf{D}^{-1} \mathrm{d}\mathbf{x}}. \tag{9}$$

Squaring both sides,

$$(\mathrm{d}t)^2 = \mathrm{d}\mathbf{x}^T \mathbf{D}^{-1} \mathrm{d}\mathbf{x}. \tag{10}$$

This last expression is quadratic in $\mathrm{d}\mathbf{x}$. Because metric tensors $\mathbf{D}$ (and $\mathbf{D}^{-1}$) must be symmetric and positive-definite, we are assured that $(\mathrm{d}t)^2 \geq 0$, and a contour of constant $\mathrm{d}t$ is an n-dimensional ellipsoid, as illustrated for $n = 2$ in Figure 2.

In 2D each symmetric positive-definite tensor

$$\mathbf{D} = \begin{bmatrix} d_{11} & d_{12} \\ d_{12} & d_{22} \end{bmatrix} \tag{11}$$

is comprised of three unique elements d_{11}, d_{12} and d_{22}. These three elements are related to the parameters for the ellipse in Figure 2 by the eigen-decomposition

$$\begin{aligned} \mathbf{D} &= \lambda_a \mathbf{a}\mathbf{a}^T + \lambda_b \mathbf{b}\mathbf{b}^T \\ \mathbf{a} &= \cos\gamma\, \mathbf{e}_1 + \sin\gamma\, \mathbf{e}_2 \\ \mathbf{b} &= -\sin\gamma\, \mathbf{e}_1 + \cos\gamma\, \mathbf{e}_2 \end{aligned} \tag{12}$$

where $\mathbf{a}$ and $\mathbf{b}$ are orthonormal eigenvectors and λ_a and λ_b their corresponding real and positive eigenvalues, ordered such that $\lambda_a \geq \lambda_b$. Equivalently,

$$\mathbf{D} = \begin{bmatrix} \lambda_a \cos^2\gamma + \lambda_b \sin^2\gamma & (\lambda_a - \lambda_b)\cos\gamma\sin\gamma \\ (\lambda_a - \lambda_b)\cos\gamma\sin\gamma & \lambda_a \sin^2\gamma + \lambda_b \cos^2\gamma \end{bmatrix}. \tag{13}$$

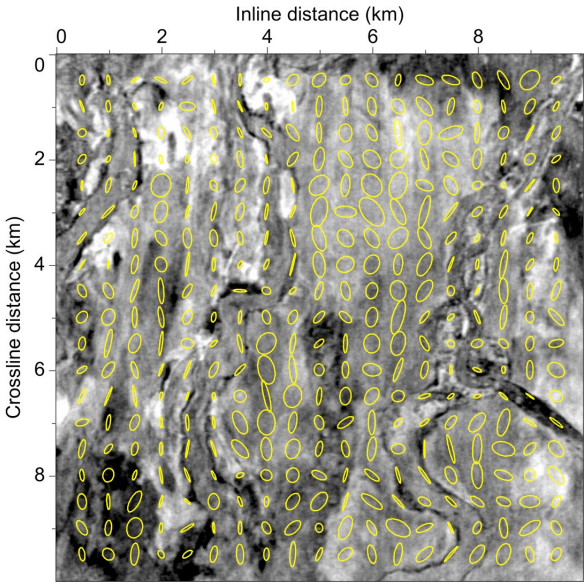

Figure 3. Ellipses for a tensor field $\mathbf{D}(\mathbf{x})$ derived from a horizontal slice of a 3D seismic image.

Equations 12 and 13 provide intuitive ways to specify a tensor field $\mathbf{D}(\mathbf{x})$ that represents an anisotropic and spatially varying model of correlation. Where correlation is high, we set both λ_a and λ_b to have large values. Where correlation is anisotropic, we set λ_a to be larger than λ_b and we choose the angle γ to be the direction in which correlation is highest. All three of the parameters λ_a, λ_b and γ may vary with location $\mathbf{x}$.

As an example, Figure 3 shows an example of tensor ellipses that represent the spatial correlation of features apparent in a 2D horizontal slice of a 3D seismic image. Correlation in this example is both anisotropic and spatially varying.

3 ON NON-PLANAR SURFACES

Now let us assume that the data to be interpolated are acquired at locations scattered on a surface defined parametrically by a mapping $\mathbf{x}(\mathbf{u}) : U \in \mathbb{R}^2 \rightarrow X \in \mathbb{R}^3$. For example, on the surface of the earth, scattered data may be acquired at locations $\mathbf{u} = (u_1, u_2)$ specified by longitude $u_1 = \phi$ and latitude $u_2 = \theta$, and each such location corresponds to a point $\mathbf{x} = (x_1, x_2, x_3)$ in a Cartesian earth-centered earth-fixed coordinate system.

Because the space X of points on the surface is a small subset of $\mathbb{R}^3$, we should not think of our scattered data as a function of $\mathbf{x}$, but rather as a function of $\mathbf{u}$. It

is most convenient to interpolate measurements in the 2D parametric space $U \in \mathbb{R}^2$ in which they are sampled.

In other words, in the blended-neighbor method of tensor-guided interpolation, we would like to first solve an eikonal equation:

$$\boldsymbol{\nabla}_u t^T \mathbf{D}_u \boldsymbol{\nabla}_u t = 1, \tag{14}$$

where $\mathbf{D}_u = \mathbf{D}_u(\mathbf{u})$ denotes a tensor field and $t = t(\mathbf{u})$ denotes non-Euclidean distance, both functions of parametric coordinates $\mathbf{u}$. This eikonal equation leads to the following question.

How should we compute the tensor field $\mathbf{D}_u(\mathbf{u})$ *so that our interpolation is consistent with both the geometry of the surface and any model of spatial correlation specified on that surface?*

Equations 12 (or 13) provide an intuitive recipe for computing metric tensors $\mathbf{D}$ in a planar coordinate space spanned by the orthonormal vectors $\mathbf{e}_1$ and $\mathbf{e}_2$. To extend this recipe to a parametric surface, we must define a similar locally planar space for every point on the surface.

3.1 The tangent space

The Jacobian $\mathbf{J}$ of the mapping $\mathbf{x}(\mathbf{u})$ is defined by

$$\mathbf{J} = [\mathbf{j}_1\ \mathbf{j}_2] = \begin{bmatrix} j_{11} & j_{12} \\ j_{21} & j_{22} \\ j_{31} & j_{32} \end{bmatrix} = \begin{bmatrix} \frac{\partial x_1}{\partial u_1} & \frac{\partial x_1}{\partial u_2} \\ \frac{\partial x_2}{\partial u_1} & \frac{\partial x_2}{\partial u_2} \\ \frac{\partial x_3}{\partial u_1} & \frac{\partial x_3}{\partial u_2} \end{bmatrix}. \tag{15}$$

The column vectors $\mathbf{j}_1$ and $\mathbf{j}_2$ of $\mathbf{J}$ are a basis for a locally planar tangent space J. In any useful surface parameterization, the vectors $\mathbf{j}_1$ and $\mathbf{j}_2$ are linearly independent; but their lengths may differ, and they need not be orthogonal. In other words, the vectors $\mathbf{j}_1$ and $\mathbf{j}_2$ illustrated in Figure 4 may not be the easiest basis in which to specify the metric tensors $\mathbf{D}$.

We can obtain a tangent space E with orthonormal basis vectors $\mathbf{e}_1$ and $\mathbf{e}_2$ by decomposition of the Jacobian matrix $\mathbf{J} = \mathbf{E}\,\mathbf{F}$:

$$\begin{bmatrix} j_{11} & j_{12} \\ j_{21} & j_{22} \\ j_{31} & j_{32} \end{bmatrix} = \begin{bmatrix} e_{11} & e_{12} \\ e_{21} & e_{22} \\ e_{31} & e_{32} \end{bmatrix} \begin{bmatrix} f_{11} & f_{12} \\ f_{21} & f_{22} \end{bmatrix}. \tag{16}$$

For example, if we choose the QR decomposition, then $\mathbf{F}$ is a right-triangular matrix with elements that can be found by Gram-Schmidt orthogonalization.

As illustrated in Figure 4, the tangent spaces J and E are really the same space, spanned by different basis vectors. In choosing the orthonormal vectors $\mathbf{e}_1$ and $\mathbf{e}_2$ (shown in Figure 2), we choose a basis for specifying a tensor field $\mathbf{D}_e$ via equation 12, rewritten here as

$$\begin{aligned} \mathbf{D}_e &= \lambda_a \mathbf{a}\mathbf{a}^T + \lambda_b \mathbf{b}\mathbf{b}^T \\ \mathbf{a} &= \cos\gamma\, \mathbf{e}_1 + \sin\gamma\, \mathbf{e}_2 \\ \mathbf{b} &= -\sin\gamma\, \mathbf{e}_1 + \cos\gamma\, \mathbf{e}_2. \end{aligned} \tag{17}$$

In using equation 17 we must remember that the orthonormal basis vectors $\mathbf{e}_1$ and $\mathbf{e}_2$ and eigenvectors $\mathbf{a}$ and $\mathbf{b}$ now have three components, as they all lie within a tangent plane in $\mathbb{R}^3$, not $\mathbb{R}^2$. In particular, the 3×2 matrix $\mathbf{E} = [\mathbf{e}_1\ \mathbf{e}_2]$ is not the identity matrix. Using the 2×2 matrix $\mathbf{D}$ defined by equation 13, equation 17 becomes

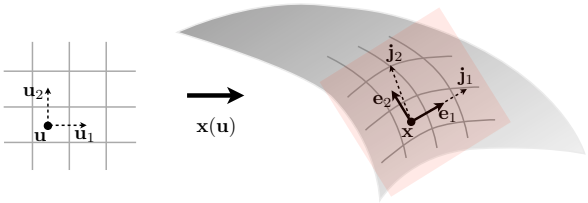

Figure 4. Unit vectors $\mathbf{u}_1$ and $\mathbf{u}_2$ are mapped to Jacobian vectors $\mathbf{j}_1$ and $\mathbf{j}_2$. These Jacobian vectors and the orthonormal basis vectors $\mathbf{e}_1$ and $\mathbf{e}_2$ lie in the plane tangent to the surface at point $\mathbf{x} = \mathbf{x}(\mathbf{u})$.

$$\mathbf{D}_e = \mathbf{E}\mathbf{D}\mathbf{E}^T \tag{18}$$

In this way we can easily specify a tensor field $\mathbf{D}_e$ for an eikonal equation

$$\boldsymbol{\nabla}_e t^T \mathbf{D}_e \boldsymbol{\nabla}_e t = 1. \tag{19}$$

To make sense of this eikonal equation in the tangent space E we must understand how to interpret the *intrinsic gradient* $\boldsymbol{\nabla}_e t$, the gradient within the tangent space.

3.2 The gradients

My interpretation of gradients follows that of Bronstein et al. (2008). In the parametric space $U \in \mathbb{R}^2$ the gradient $\boldsymbol{\nabla}_u t$ has two components

$$\boldsymbol{\nabla}_u t = \begin{bmatrix} \frac{\partial t}{\partial u_1} \\ \frac{\partial t}{\partial u_2} \end{bmatrix}, \tag{20}$$

and in the Cartesian space $X \in \mathbb{R}^3$ the *extrinsic gradient* $\boldsymbol{\nabla}_x t$ has three components

$$\boldsymbol{\nabla}_x t = \begin{bmatrix} \frac{\partial t}{\partial x_1} \\ \frac{\partial t}{\partial x_2} \\ \frac{\partial t}{\partial x_3} \end{bmatrix}. \tag{21}$$

The parametric and extrinsic gradients are simply related by the chain rule for differentiation,

$$\frac{\partial t}{\partial u_j} = \frac{\partial x_1}{\partial u_j}\frac{\partial t}{\partial x_1} + \frac{\partial x_2}{\partial u_j}\frac{\partial t}{\partial x_2} + \frac{\partial x_3}{\partial u_j}\frac{\partial t}{\partial x_3}, \tag{22}$$

for $j = 1, 2$, so that

$$\boldsymbol{\nabla}_u t = \mathbf{J}^T \boldsymbol{\nabla}_x t = \mathbf{F}^T \mathbf{E}^T \boldsymbol{\nabla}_x t. \tag{23}$$

In any coordinate space, the gradient of a scalar field t is defined to be the vector $\boldsymbol{\nabla} t$ for which the dot product $\boldsymbol{\nabla} t^T \mathbf{v}$ equals the directional derivative

$$D_v t(\mathbf{x}) \equiv \lim_{\epsilon \to 0} \frac{t(\mathbf{x} + \epsilon \mathbf{v}) - t(\mathbf{x})}{\epsilon}, \tag{24}$$

for every vector $\mathbf{v}$ in the space. If that vector $\mathbf{v}$ is confined to the tangent space E, then using

$$t(\mathbf{x}+\epsilon\mathbf{v}) = t(\mathbf{x}) + \epsilon[\boldsymbol{\nabla}_x t(\mathbf{x})]^T\mathbf{v} + O(\epsilon^2), \tag{25}$$

we have

$$\boldsymbol{\nabla}_e t^T\mathbf{v} = \boldsymbol{\nabla}_x t^T\mathbf{v}. \tag{26}$$

For this equation to be satisfied for every vector $\mathbf{v}$ in the tangent space E, the intrinsic gradient $\boldsymbol{\nabla}_e t$ must be the projection of the extrinsic gradient $\boldsymbol{\nabla}_x t$ onto the tangent plane at location $\mathbf{x}$ on the surface.

This observation is the key to finding a relationship between the intrinsic gradient $\boldsymbol{\nabla}_e t$ and the parametric gradient $\boldsymbol{\nabla}_u t$. We have equation 23 relating $\boldsymbol{\nabla}_u t$ and $\boldsymbol{\nabla}_x t$. If we can find a relationship between $\boldsymbol{\nabla}_e t$ and $\boldsymbol{\nabla}_x t$, then we can express $\boldsymbol{\nabla}_e t$ in terms of $\boldsymbol{\nabla}_u t$, and we will know how to compute $\mathbf{D}_u$ (in equation 14) in terms of $\mathbf{D}_e$.

The intrinsic gradient $\boldsymbol{\nabla}_e t$ in the tangent space E can be written as $\boldsymbol{\nabla}_e t = \mathbf{E}\,\mathbf{c}$ for some coefficients in a vector $\mathbf{c}$ that define the projection of $\boldsymbol{\nabla}_x t$ onto E. The coefficients $\mathbf{c}$ are the least-squares solution of $\mathbf{E}\,\mathbf{c} \approx \boldsymbol{\nabla}_x t$:

$$\begin{aligned}\mathbf{E}^T\mathbf{E}\,\mathbf{c} &= \mathbf{E}^T\boldsymbol{\nabla}_x t \\ \mathbf{c} &= \mathbf{E}^T\boldsymbol{\nabla}_x t\end{aligned} \tag{27}$$

so that

$$\boldsymbol{\nabla}_e t = \mathbf{E}\mathbf{E}^T\boldsymbol{\nabla}_x t. \tag{28}$$

Here I have used the fact that the columns $\mathbf{e}_1$ and $\mathbf{e}_2$ of $\mathbf{E}$ are orthonormal vectors, so that $\mathbf{E}^T\mathbf{E} = \mathbf{I}$.

3.3 The parametric tensor field

Combining equations 23 and 28, we can express the intrinsic gradient in terms of the parametric gradient:

$$\boldsymbol{\nabla}_e t = \mathbf{E}\mathbf{F}^{-T}\boldsymbol{\nabla}_u t. \tag{29}$$

so that the eikonal equation 14 becomes

$$\boldsymbol{\nabla}_u t^T\mathbf{F}^{-1}\mathbf{E}^T\mathbf{D}_e\mathbf{E}\mathbf{F}^{-T}\boldsymbol{\nabla}_u t = 1. \tag{30}$$

Comparing this equation with equation 14 in parametric coordinates, we find

$$\mathbf{D}_u = \mathbf{F}^{-1}\mathbf{E}^T\mathbf{D}_e\mathbf{E}\mathbf{F}^{-T} \tag{31}$$

or, using equation 18,

$$\mathbf{D}_u = \mathbf{F}^{-1}\mathbf{D}\mathbf{F}^{-T}. \tag{32}$$

$\mathbf{D}_u$ is the tensor field needed to specify the eikonal equation 14 in parametric coordinates. It is the answer to the question asked above. The matrices $\mathbf{F}^{-1}$ and $\mathbf{F}^{-T}$ account for surface geometry, and the 2×2 matrix $\mathbf{D}$ sandwiched between them represents a model of spatial correlation that may be anisotropic and may vary with location on the surface. Note that this matrix $\mathbf{D}$ is exactly the same as that in equation 13, used to represent correlation for 2D interpolation within a plane. Here the matrix $\mathbf{D}$ describes correlation within a local tangent plane.

As a special case, if our model for spatial correlation on the surface is isotropic and constant (perhaps because we have no secondary information to the contrary), then $\mathbf{D} = \mathbf{I}$ and

$$\mathbf{D}_u = \left(\mathbf{F}^T\mathbf{F}\right)^{-1}. \tag{33}$$

Distances $t(\mathbf{u})$ are then simply geodesic distances computed by solution of

$$\boldsymbol{\nabla}_u t^T\left(\mathbf{F}^T\mathbf{F}\right)^{-1}\boldsymbol{\nabla}_u t = 1. \tag{34}$$

In this special case, the tensor field $\mathbf{D}_u(\mathbf{u})$ accounts for only the geometry of the surface. Again, because the matrix $\mathbf{F}^T\mathbf{F}$ is symmetric and positive-definite, each tensor can be represented by an ellipse, as in Figure 2.

4 THE EARTH'S SURFACE

As a simple example, let us consider the parametric mapping $\mathbf{x}(\mathbf{u})$ illustrated in Figure 5. A simple approximation of the earth's surface is a sphere with constant radius r, for which an equirectangular parametric mapping is

$$\begin{aligned}x_1 &= r\cos\phi\cos\theta \\ x_2 &= r\sin\phi\cos\theta \\ x_3 &= r\sin\theta.\end{aligned} \tag{35}$$

The parameters are longitude $u_1 \equiv \phi$ and latitude $u_2 \equiv \theta$. For this example, the orthonormal basis vectors $\mathbf{e}_1$ and $\mathbf{e}_2$ represent easting and northing, respectively, and the matrix $\mathbf{F}$ is

$$\mathbf{F} = \begin{bmatrix} r\cos\theta & 0 \\ 0 & r \end{bmatrix}. \tag{36}$$

Then, assuming that spatial correlation is isotropic and constant on the earth's surface (so that $\mathbf{D} = \mathbf{I}$),

$$\mathbf{D}_u = \begin{bmatrix} \frac{1}{r^2\cos^2\theta} & 0 \\ 0 & \frac{1}{r^2} \end{bmatrix}. \tag{37}$$

Because the matrix $\mathbf{D}_u$ is diagonal, its effect is to simply scale the coordinate axes in the parametric space U so that equation 34 becomes

$$\frac{1}{r^2\cos^2\theta}\left(\frac{\partial t}{\partial\phi}\right)^2 + \frac{1}{r^2}\left(\frac{\partial t}{\partial\theta}\right)^2 = 1, \tag{38}$$

which is simply the eikonal equation in spherical coordinates, omitting any gradient with respect to radius r, because r is constant on the surface. Times $t(\phi,\theta)$ computed by solving this equation are geodesic great-circle distances.

The advantage of the more general eikonal equation 14, with tensor field $\mathbf{D}_u$ defined by equation 32, is that we can specify an additional tensor field $\mathbf{D}$ representing a model for correlation that varies with location on the surface of the Earth.

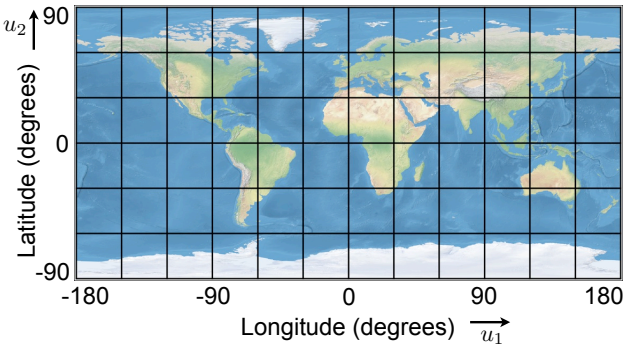

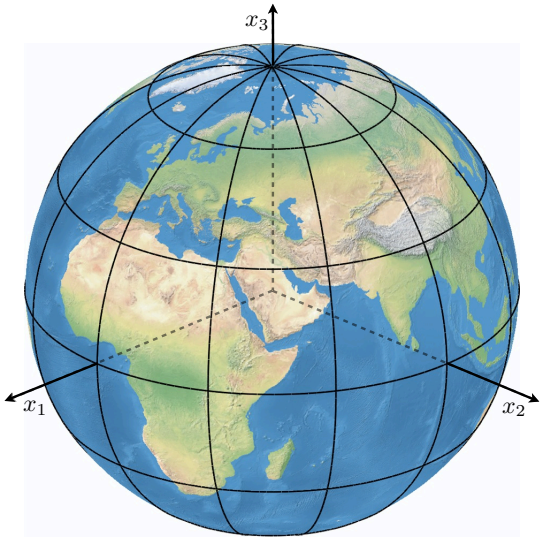

Figure 5. Parametric (equirectangular) mapping of the earth's surface.

4.1 Atmospheric CO_2 concentrations

As an example of data recorded on the earth's surface, Figure 6 shows monthly averages for April, 2009, of atmospheric CO_2 concentrations, measured in flasks at 65 locations scattered around the globe. These data are made publicly available (ftp://ftp.cmdl.noaa.gov) by the National Oceanic and Atmospheric Administration (NOAA). CO_2 concentrations are expressed as mole fractions, in parts per million.

To use blended neighbor interpolation as defined by equations 4 and 5 in the parametric longitude-latitude space U, we must provide a tensor field $\mathbf{D}_u(\mathbf{u})$. If we simply assume that spatial correlation is isotropic and constant on the earth's surface, then the tensors are given by equation 37. Of course, this simple assumption is unnecessary, because equation 32 can include any tensor field $\mathbf{D}(u)$ defined within local tangent planes on the earth's surface. What secondary information can help us define this tensor field $\mathbf{D}(\mathbf{u})$?

Variation with latitude of solar radiation suggests that CO_2 concentrations are likely to vary more in the

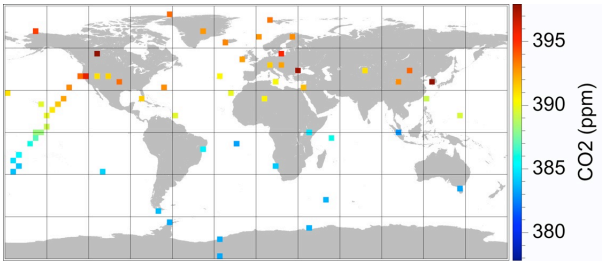

Figure 6. Averages of atmospheric CO_2 concentrations measured at 65 scattered locations on the earth's surface in April, 2009.

north-south direction than in the east-west direction. Such anistropy in spatial correlation can be seen in satellite images of CO_2 concentrations in the middle troposphere, provided by the Atmospheric Infrared Sounder (AIRS) mission of the National Aeronautics and Space Administration (NASA). We might use these images to compute anisotropic and spatially-varying tensors $\mathbf{D}$ like those computed from the seismic image shown in Figure 3. Alternatively, we might use atmospheric transport models to derive these tensors. Unlike methods that assume stationarity, the blended neighbor interpolation method can be used for arbitrary tensor fields.

For this example, however, I chose a simpler stationary model of spatial correlation; everywhere on the earth's surface, I use the tensor

$$\mathbf{D} = \begin{bmatrix} 1 & 0 \\ 0 & \frac{1}{16} \end{bmatrix}. \tag{39}$$

The aspect ratio for the corresponding tensor ellipse is 4:1, which implies a correlation distance that is four times higher in the east-west direction than in the north-south direction.

In developing this simple model, I computed variograms for the 65 CO_2 measurements displayed in Figure 6. Figure 7 shows two such variograms. Each was computed for geodesic (great-circle) distances in bins with widths of 10 degrees. The value for each bin is the rms difference of values for pairs of CO_2 measurements that are separated by the distances for that bin in the east-west and north-south directions.

Figure 7a shows that differences in CO_2 values tend to be smaller for measurements at stations that are nearby, and that these differences increase more rapidly in the north-south direction than in the east-west direction. The ellipse superimposed on this variogram has an aspect ratio of 4:1, and is roughly a contour of constant deviation or correlation.

Figure 7b displays a variogram computed in the same way, after a random permutation of only the CO_2 values, not the station locations. No increase (or decrease) in deviation with distance is apparent in this variogram. Deviations for small distances tend toward the middle of the range of deviations shown, and tend to vary less than those for larger distances, simply because

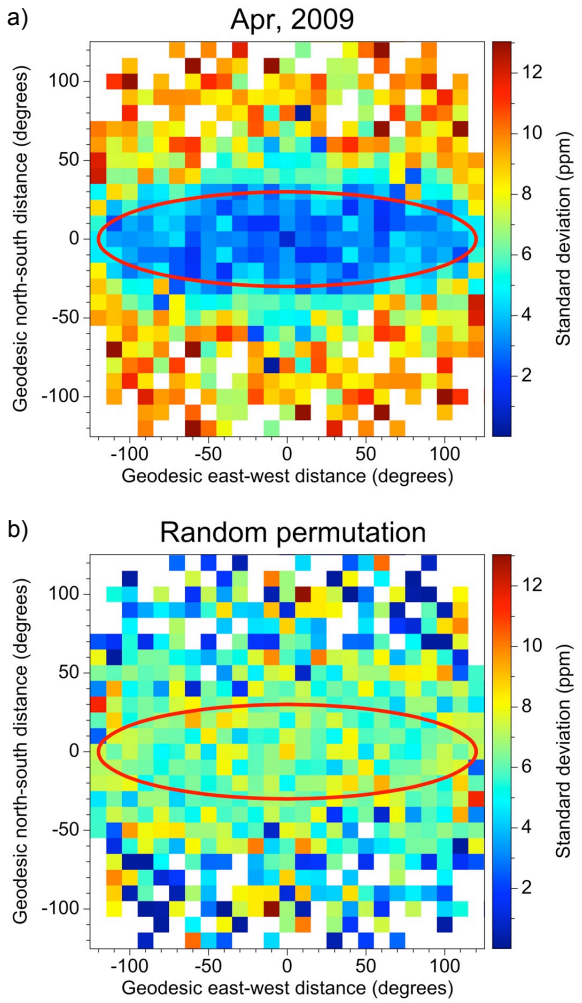

Figure 7. A variogram (a) computed for atmospheric CO_2 concentrations measured at 65 scattered locations on the earth's surface and (b) for a random permutation of those same measurements. The ellipse has an aspect ratio of 4:1.

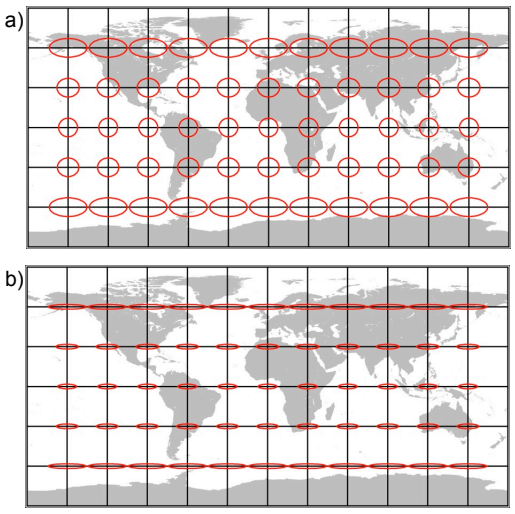

Figure 8. Two tensor fields defined for the surface of the earth. One tensor field (a) is isotropic on the earth spheroid The other (b) is anisotropic on the earth spheroid, and implies less correlation with distance in the north-south direction than in the east-west direction.

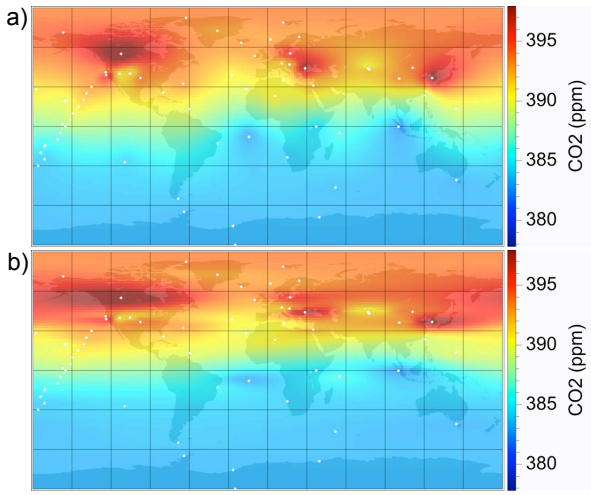

Figure 9. Tensor-guided interpolations of CO_2 concentrations for the (a) isotropic and (b) anisotropic tensor fields displayed in Figure 8.

the bins for smaller distances contain more values from which rms differences are computed. Deviations for bins at larger distances are both lower and higher and are less consistent because fewer values contribute to each bin. This variogram of permuted values implies that the spatial correlation apparent in Figure 7a is significant.

Figure 8 displays two tensor fields, which correspond to spatial correlation models that are isotropic (Figure 8a) and anisotropic (Figure 8b) on the surface of the earth. Note that both tensor fields are anisotropic and spatially varying in the parametric space of longitude and latitude. However, on the curved surface of the earth, the tensors displayed in Figure 8a would appear circular and identical, while those in Figure 8b would appear elliptical and identical.

Figure 9 displays the corresponding tensor-guided blended neighbor interpolations. The interpolation in Figure 9b is the same as that displayed in Figures 1b and 1c. As expected, contours of constant CO_2 concentration in Figure 9a are more circular, more isotropic, than those in Figure 9b. The increase in east-west correlation of CO_2 concentrations apparent in Figure 9b is consistent with the anisotropic tensor field in Figure 8b and the variogram in Figure 7a.

5 CONCLUSION

The example in the previous section demonstrates that the blended neighbor interpolation method can easily account for an anisotropic model of spatial correlation on the earth's surface. However, geostatistical methods for interpolation, such as kriging, can do this as well for special surface geometries, such as a sphere.

A distinguishing feature of the blended neighbor method is its ability to honor non-stationary models of spatial correlation. These may reflect more general (non-spherical) surface geometries, such as seismic horizons, as well as spatial correlation apparent in secondary data, such as seismic or satellite images. More general and non-stationary models violate fundamental assumptions made by most geostatistical interpolation methods. Such models are therefore seldom used today, but are easily handled by blended neighbor interpolation.

REFERENCES

Bronstein, A., M. Bronstein, and R. Kimmel, 2008, Numerical geometry of non-rigid shapes, 1st ed.: Springer.

Gurney, K., R. M. Law, A. S. Denning, P. J. Rayner, D. Baker, P. Bousquet, L. Bruhwiler, Y.-H. Chen, P. Ciais, S. Fan, I. Y. Fung, M. Gloor, M. Heimann, K. Higuchi, J. John, T. Maki, S. Maksyutov, K. Masarie, P. Peylin, M. Prather, B. C. Pak, J. Randerson, J. Sarmiento, S. Taguchi, T. Takahashi, and C.-W. Yuen, 2002, Towards robust regional estimates of CO2 sources and sinks using atmospheric transport models: Nature, **415**, 626–630.

Hale, D., 2009, Image-guided blended neighbor interpolation of scattered data: 79th Annual International Meeting, SEG, Expanded Abstracts, 1127–1131.

Lee, R., 2001, Pitfalls in seismic data flattening: The Leading Edge, **20**, 160–164.

Peters, W., A. Jacobson, C. Sweeney, A. Andrews, T. Conway, K. Masarie, J. Miller, L. Bruhwiler, G. Pétron, A. Hirsch, D. Worthy, G. van der Werf, J. Randerson, P. Wennberg, M. Krol, and P. Tans, 2007, An atmospheric perspective on North American carbon dioxide exchange: CarbonTracker: Proceedings of the National Academy of Sciences, **104**, 18925–18930.